Available online at www.sciencedirect.com
ScienceDirect
Trans. Nonferrous Met. Soc. China 32(2022) 1969−1980
Transactions of Nonferrous Metals Society of China
www.tnmsc.cn

Hydrogen storage properties of Mg(Al) solid solution alloy doped with LaF_3 by ball milling

Hai-chang ZHONG[1], Chen-long LIN[1], Zi-yu DU[1], Chun-yan CAO[1], Chu LIANG[2], Qing-rong ZHENG[3], Le-yang DAI[3]

1. Fujian Provincial Key Laboratory of Functional Materials and Applications, School of Materials Science and Engineering, Xiamen University of Technology, Xiamen 361024, China;
2. College of Materials Science and Engineering, Zhejiang University of Technology, Hangzhou 310014, China;
3. Fujian Provincial Key Laboratory of Naval Architecture and Ocean Engineering, School of Marine Engineering, Jimei University, Xiamen 361021, China

Received 31 May 2021; accepted 14 January 2022

Abstract: LaF_3 was doped to the Mg(Al) solid solution alloy for enhancing the hydrogen absorption and desorption by ball milling. XRD was used to analyze the phases of the samples and the phase transition induced by hydrogenation and dehydrogenation. The microstructure and phase distribution were investigated by SEM and STEM. The hydrogen storage properties were measured by Sieverts method. For $Mg_{0.93}Al_{0.07}$−5wt.%LaF_3 nanocomposite, the hydrogen storage kinetic properties were significantly improved by reducing the hydriding and dehydriding activation energies to 65 and 78 kJ/mol, respectively, and the dehydriding enthalpy was calculated to be 69.7 kJ/mol. The improved hydrogen storage properties were mainly attributed to the catalytic effects of the in situ formed nanostructure $Al_{11}La_3$ and MgF_2 together with the dissolving of Al in Mg lattice.

Key words: lanthanum fluorite; magnesium hydride; magnesium; aluminum; hydrogen storage properties; hydrogenation

1 Introduction

Hydrogen storage is the bottleneck of hydrogen economy [1,2]. Solid state hydrogen storage based on metal hydrides is an amazing method possible to solve the problem for the superiorities in safety and convenience [1]. MgH_2 is one of the most promising hydrogen storage materials due to the outstanding advantages, including high capacity (7.6 wt.%), good cyclic stability, low price, and so on [3]. Unfortunately, MgH_2 needed a high temperature over 300 °C to release hydrogen for the high thermodynamic stability and large reaction energy barriers [4−7]. In the past decades, great progresses have been achieved on the improvement of hydrogen storage properties [8,9], but still not satisfying the practical utilization. Therefore, it is necessary to make more efforts to improve the hydrogen absorption and desorption of Mg.

Alloying with the metallic elements (Ni, Cu, Al, etc) is an extensively used strategy to modulate the hydrogen storage property of Mg [3,10−13]. Mg_2Ni is a typical alloy which reversibly absorbs 3.6 wt.% H_2 with dehydriding enthalpy of 64 kJ/mol [14]. It was confirmed that the dehydriding/hydriding kinetics and the thermodynamics of Mg could be altered by alloying with Ni [15,16]. Among the alloying elements, Al is a fascinating one for improving the hydrogen storage property of Mg. It was found that $Mg_{17}Al_{12}$ and

Corresponding author: Hai-chang ZHONG, Tel: +86-592-6291337, E-mail: hczhong@xmut.edu.cn;
Le-yang DAI, Tel: +86-592-6186831, E-mail: daileyang@jmu.edu.cn
DOI: 10.1016/S1003-6326(22)65923-5

Al_3Mg_2 could promote the hydrogenation and dehydrogenation of Mg [17−19]. The dehydriding enthalpy of MgH_2 could be lowered by the exothermic formation of $Mg_{17}Al_{12}$ and/or Al_3Mg_2 [20]. Different from the ever reports, we also found that the dehydrogenation/hydrogenation of Mg could be improved by dissolving of Al [5]. But the hydrogen storage properties of Mg(Al) solid solution alloys, especially the kinetics, deteriorated fast due to the agglomeration of Al.

Doping catalysts, which is an effective way to improve the kinetics, such as transition metals [10,21,22], metal fluorites [23,24], metal oxides [25], and rare earths (Y, La, Ce) [26,27], was used to enhance the dehydriding/hydriding kinetics. Among the transition metals, Ti is more effective in enhancing the hydrogenation, but V is the optimal catalyst on accelerating the dehydrogenation [22]. The catalytic effects of the transition metals were mainly attributed to their special 3d orbit structures or forming unstable hydrides [28,29]. Some high valence transition metal oxides, such as Cr_2O_3 and TiO_2, were also found to be good catalysts [30,31]. It was demonstrated that TiO_2 had superior catalytic effects than Ti [32]. To obtain more effective catalyst, Al-based compounds were newly designed to improve the hydrogen storage properties of Mg-based alloys [33]. For example, the dehydriding activation energy of $Mg@Mg_{17}Al_{12}$ nanocomposite was reduced to 44.7 kJ/mol by doping with AlV_3 [34]. Al_2Ti was confirmed to enhance the dehydrogenation of MgH_2 by promoting the nucleation of Mg [35]. Pr_3Al_{11} was reported not only enhancing the hydrogen storage kinetics, but also acting as inhibitor to the growth of Mg/MgH_2 nanocrystalline [27]. In the present work, we designed $Mg_{0.93}Al_{0.07}$−5wt.%LaF_3 nanocomposite to improve the hydrogen storage performances. It was originally reported that the in situ formed nanostructure $Al_{11}La_3$ combining with MgF_2 improved the dehydriding/hydriding kinetics, and inhibited the agglomeration of Al, thus improving the dehydriding/hydriding stability. The results provide a simple strategy to improve the hydrogen storage properties of Mg-based alloys.

2 Experimental

The commercial Mg and Al (99.9%, ~45 μm, purchased from Zhongnuo Advanced Material (Beijing) Technology Co., Limited, China), were used as starting materials for the preparation of Mg(Al) solid solution alloy. Sample with composition of Mg−7at.%Al ($Mg_{0.93}Al_{0.07}$) was synthesized by mechanical alloying. The weighed Mg and Al powder mixture was sealed in the stainless steel vials together with the stainless steel balls (1:50, mass ratio), and transferred to a planetary miller (QM−3SP2) to perform mechanical alloying. The duration of mechanical alloying was 70 h until the formation of Mg(Al) solid solution alloy. The details of mechanical alloying were reported in our previous work [5]. Then, 5 wt.% LaF_3 (ALFA, 99.9%, ~45 μm) was added to the $Mg_{0.93}Al_{0.07}$ alloy by ball milling for 20 h to synthesize a nanocomposite ($Mg_{0.93}Al_{0.07}$−5 wt.%LaF_3). To avoid oxidation, all handlings were carried out in a glove box filled with high purity argon.

Phase analysis was performed on an X-ray diffractometer (XRD, Rigaku SmartLab 2 kW, Japan) equipped with Cu K_α radiation (λ=1.54056 Å). The XRD data were collected in the 2θ range from 15° to 85° with a scanning rate of 2 (°)/min. Field emission scanning electron microscope (SEM, ZEISS Sigma 500 attached OXFORD X-Max^N EDS) and scanning transmission electron microscope (STEM, FEI TALOS F200S attached BRUKER Super-X EDS) were used to observe the microstructure and the phase distribution. The dehydriding/hydriding performances were measured by Sieverts method on the automatic equipment. $Mg_{0.93}Al_{0.07}$−5wt.%LaF_3 (0.200 g) nanocomposite was precisely weighed and sealed in a small sample holder, then loaded into a stainless steel vessel for the measurement of hydrogen storage properties. Before the measurement, the pipelines and sample chamber were evacuated about 30 min, then the volume of sample chamber at room temperature and target temperature were calibrated four times using high purity argon by the program. The average value of four times was used as the final volume for the following hydrogen storage measurements. To achieve stable hydrogen absorption and desorption performances, the sample firstly underwent five dehydriding/hydriding cycles at 300 °C. Then, the isothermal hydrogen absorption and desorption, and the pressure−composition isothermal (PCI) measurements were carried out automatically

according to the pre-set program. For the isothermal hydrogen absorption, the initial hydrogen pressure was set to be 2.5 MPa, and the isothermal hydrogen desorption started from about 1×10^{-4} MPa. The PCI measurements were carried out following the kinetic measurement.

3 Results and discussion

3.1 Microstructure and dehydrogenation/hydrogenation inducing phase transitions

Figure 1 shows XRD patterns of $Mg_{0.93}Al_{0.07}$−5wt.%LaF_3 nanocomposite at different states. Figure 1(a) shows the ball-milled $Mg_{0.93}Al_{0.07}$−5wt.%LaF_3 nanocomposite. Except for the original Mg(Al) solid solution and the additive of LaF_3, there was no other phase observed, indicating that LaF_3 did not react with Mg(Al) solid solution alloy during the ball milling process. The visible broadening of the diffraction peaks of Mg indicates the grain refinement by ball milling. The average grain size was calculated to be about 27 nm by Scherrer method using the full width at half maximum of $Mg(10\bar{1}1)$ peak. In fact, there were lots of smaller grains. The results indicated that the addition of Al and LaF_3 promoted the grain refinement of Mg. The cell parameters (a and c) of Mg were gotten to be about 0.31928(4) and 0.51877(1) nm, respectively, which were close to the previous results [5], showing the formation of Mg(Al) solid solution. Figure 1(b) shows the hydrogenated $Mg_{0.93}Al_{0.07}$−5wt.%LaF_3 nanocomposite, in which MgH_2, intermetallic compound $Al_{11}La_3$, MgF_2 and Al species, were all confirmed. Comparing Fig. 1(a) with Fig. 1(b), it could be concluded that Mg(Al) solid solution took a disproportionation reaction by hydrogenation, and reacted with LaF_3 transiting to the phases as observed in Fig. 1(b). Figure 1(c) shows the XRD pattern of the dehydrogenated $Mg_{0.93}Al_{0.07}$−5wt.%LaF_3 nanocomposite, showing that $Al_{11}La_3$ and MgF_2 were not decomposed; however, the element Al was re-dissolved into Mg lattice by dehydrogenation. Based on our previous work, Mg(Al) solid solution alloys could be hydrogenated to MgH_2 and $Mg_{17}Al_{12}$, the latter transformed to MgH_2 and Al_3Mg_2, finally Al_3Mg_2 changed to MgH_2 and Al at higher hydrogen pressure, and the dehydrogenation was just the other way round [5]. However, in this work, $Mg_{17}Al_{12}$ and Al_3Mg_2 were not found in the hydrogenated and dehydrogenated $Mg_{0.93}Al_{0.07}$−5wt.%LaF_3 nanocomposite. The reason could be that LaF_3 reacted with Al (from the decomposition of $Mg_{0.93}Al_{0.07}$ solid solution alloy), forming $Al_{11}La_3$. On the other hand, the distribution of the residual Al was highly improved as discussed below, which benefited to the reaction of MgH_2 and Al transiting to Mg(Al) solid solution by dehydrogenation. It was clear that the dehydriding/hydriding reaction of $Mg_{0.93}Al_{0.07}$−5wt.%LaF_3 nanocomposite was different with the $Mg_{0.93}Al_{0.07}$ solid solution alloy [5]. So, it is reasonable to conclude that the addition of LaF_3 changes the dehydriding/hydriding mechanism of $Mg_{0.93}Al_{0.07}$ solid solution alloy.

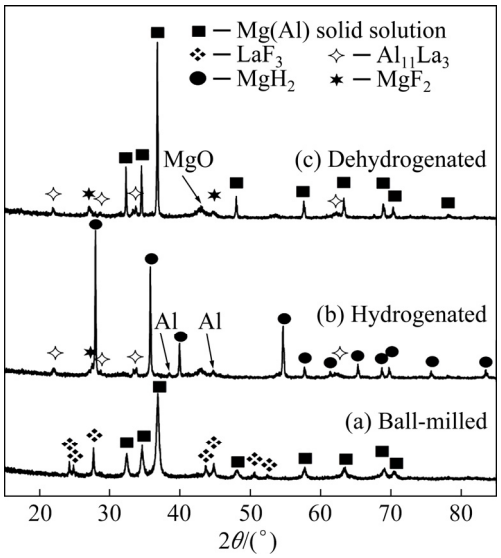

Fig. 1 XRD patterns showing phases and phase transition of $Mg_{0.93}Al_{0.07}$−5wt.%LaF_3 nanocomposite upon dehydrogenation/hydrogenation

The microstructure and phase distribution were further investigated by SEM and STEM. As shown in Fig. 2(a), the ball-milled $Mg_{0.93}Al_{0.07}$−5wt.%LaF_3 nanocomposite was irregular particles with submicron in dimension. Actually, the large particles were assembled by lots of much smaller particles as seen in Figs. 2(g) and (h). This was a typical irregular submicron particle morphology induced by ball milling. As expected, the doped LaF_3 (light particles pointed by the arrows) was homogeneously dispersed in the surface and/or body of Mg(Al) solid solution alloy particles, as illustrated in Fig. 2(b) (back scattering electron image). The element mapping analysis (Figs. 2(c, d)) further confirmed the LaF_3 and its distribution.

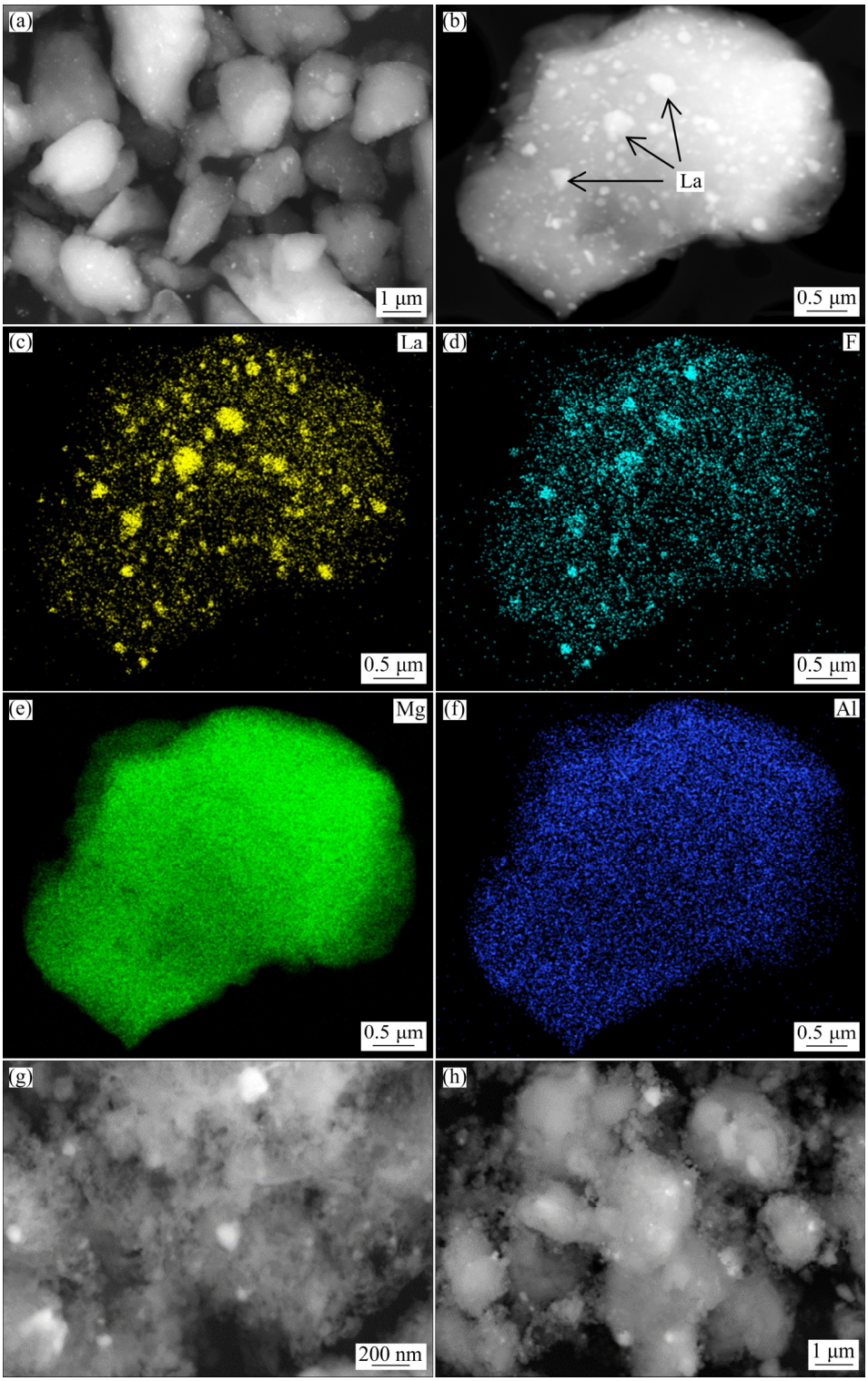

Fig. 2 SEM images (a, b, g, h) and element distribution (c−f) of $Mg_{0.93}Al_{0.07}$−5wt.%LaF_3 nanocomposite at different states: (a−f) Ball-milled; (g) Hydrogenated; (h) Dehydrogenated

Figures 2(g) and (h) are the enlarged morphologies of hydrogenated and dehydrogenated $Mg_{0.93}Al_{0.07}$−5wt.%LaF_3 nanocomposite, respectively. Obviously, the particles were broken by hydrogenation, but they assembled again during the dehydring process. The nanostructure $Al_{11}La_3$ was stable in the MgH_2/Mg matrix, which was consistent with the above XRD analysis. The selected area electron diffraction (Fig. 3(a)) and the element analysis (Figs. 3(c, d)) further confirmed the existence of

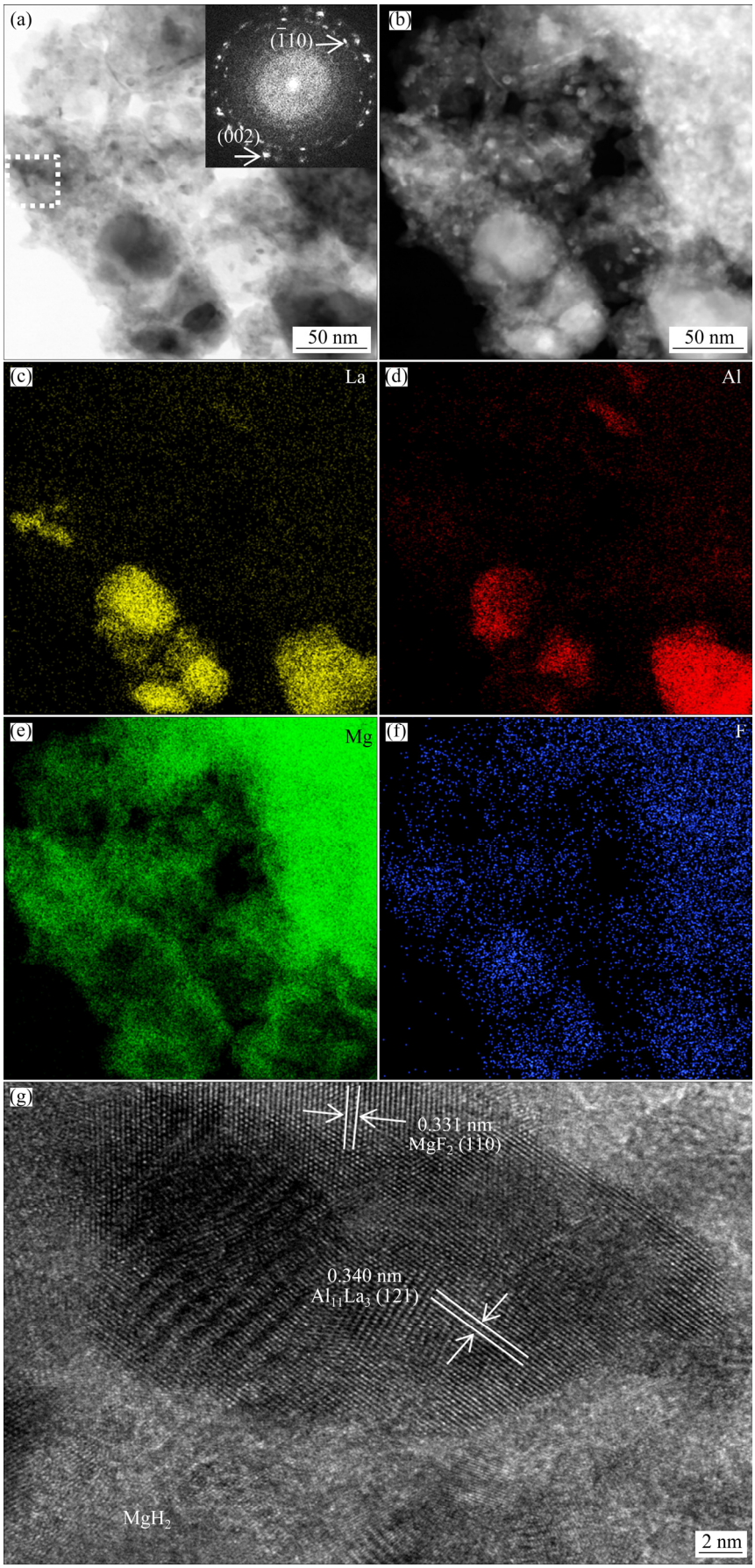

Fig. 3 Microstructure (a, b), element distribution (c−f) and phase distribution (g) of hydrogenated $Mg_{0.93}Al_{0.07}$−5wt.%LaF_3 nanocomposite obtained by STEM

$Al_{11}La_3$. $Al_{11}La_3$ was polycrystalline with nano-structure, and surrounded by nano-MgH_2 as observed in Fig. 3(b). The high resolution STEM (Fig. 3(g)) further indicated that the intermetallic compound $Al_{11}La_3$ was symbiotic with the nano-MgH_2, and there was nanostructure MgF_2 on the surfaces or at interfaces. The nanostructure $Al_{11}La_3$ and MgF_2 dispersed in Mg/MgH_2 matrix could act as the inhibitor to the agglomeration and growth of the nano-Mg/MgH_2. However, the Al species were not observed by SEM and STEM. It could be found that Al was ultrafine and highly dispersed in the MgH_2 matrix.

3.2 Dehydriding/hydriding kinetics

The isothermal hydrogen absorption and desorption curves of $Mg_{0.93}Al_{0.07}$−5wt.%LaF_3 nanocomposite are illustrated in Fig. 4. The maximum hydrogen content was 6.2 wt.%, and did not change with the temperature, indicating that $Mg_{0.93}Al_{0.07}$−5wt.%LaF_3 composite was easy to be completely hydrogenated. From Fig. 4(a) it could be seen that the activated $Mg_{0.93}Al_{0.07}$−5wt.%LaF_3 nanocomposite absorbed 5.6 wt.% H_2 (~90% of the capacity) in 10 min at 260 °C, and finished hydrogen absorption in 5 min when hydrogenated at 320 °C. However, the un-doped $Mg_{90}Al_{10}$ alloy needed more than 20 min to absorb 5.0 wt.% H_2 at 335 °C [5]. And it was reported that the ball-milled and cast $Mg_{90}Al_{10}$ alloy needed more than 100 min to finish hydrogen absorption at 380 °C, but greatly improved by the addition of nano-CeO_2 [36,37]. Figure 4(b) shows the corresponding hydrogen desorption kinetic curves. Obviously, the temperature had remarkable influence on the hydrogen desorption rate. It took about 30 min to complete hydrogen desorption at 260 °C. But the hydrogen desorption time was decreased to about 10 min at 320 °C. The hydrogen desorption rate was obviously lower than the hydrogen absorption rate. But the $Mg_{0.93}Al_{0.07}$−5wt.%LaF_3 nanocomposite exhibited improved hydrogen desorption property than the ball-milled and cast $Mg_{90}Al_{10}$ alloy [36], similar to the nano-Ni catalyzed $Mg_{90}Al_{10}$ alloy [21]. Interestingly, the dehydriding/hydriding kinetics had no visible deterioration after more than 20 cycles of hydrogen absorption and desorption for $Mg_{0.93}Al_{0.07}$−5wt.%LaF_3 nanocomposite, indicating a good dehydriding/hydriding stability. The improved dehydriding/hydriding cycling performance could be mainly attributed to the high structural stability owing to the in situ formed nanostructure $Al_{11}La_3$ and MgF_2 acting as the inhibitor to the growth of nano-Mg/MgH_2 and the agglomeration of elemental Al.

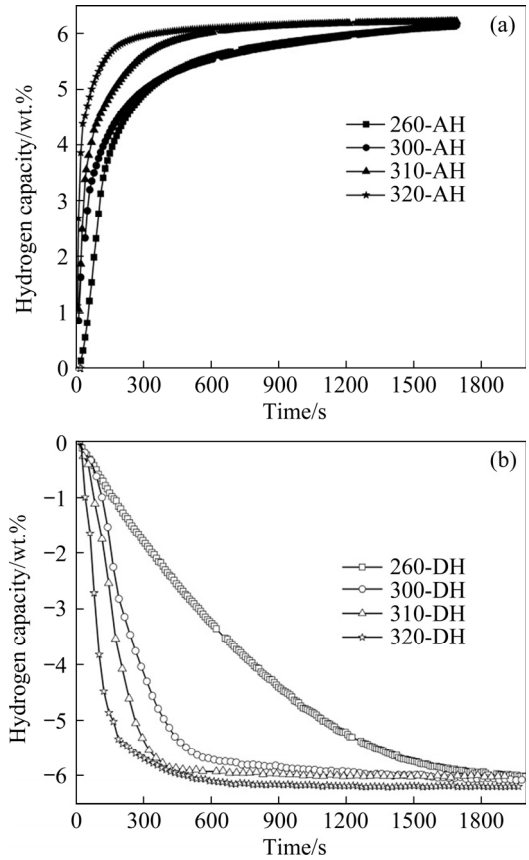

Fig. 4 Isothermal hydrogen absorption (a) and desorption (b) curves (AH: Absorbed hydrogen, DH: Desorbed hydrogen)

The dehydriding/hydriding kinetics (Fig. 4) was further analyzed by the theoretical model for understanding the mechanism upon the improvement of kinetics. As a type of gas-solid state reaction based on the nucleation-growth reaction mode, the Johnson−Mehl−Avrami−Kolmogorov (JMAK) theoretical model is considered to be more suitable for the investigation on the dehydriding/hydriding kinetics of Mg and Mg-based alloys [35]. In the present work, the linear form of JMAK equation (Eq. (1)) was used to fit the kinetics data (Fig. 4).

$$\ln[-\ln(1-\alpha)]=\eta\ln k+\eta\ln t \quad (1)$$

where α is the reaction fraction (It took the value of C_t/C in this work, C_t is the hydrogen content when the reaction proceeds to time t, C is the maximum

hydrogen content), k is the reaction rate constant, and η is the reaction exponent (or Avrami exponent). Generally, it is regarded that the result is more reliable for JMAK theoretical model in the condition of $\alpha < 0.5$. So, the starting linear part of the reaction fraction to time on the kinetics curve ($\alpha < 0.5$) was chosen for the fitness. The fitting results are shown in Fig. 5(a) and Fig. 6(a) for the hydrogen absorption and desorption, respectively. From Fig. 5(a) and Fig. 6(a), the temperature-dependent k values were achieved, and further used to calculate the apparent activation energy (E_a) by the Arrhenius equation (Eq. (2)):

$$\ln k = -\left(\frac{E_a}{RT}\right) + K \tag{2}$$

where K is a temperature-independent coefficient, R is the molar gas constant (8.31 J/(mol·K)), and T is the thermodynamic temperature. The Arrhenius calculation results are illustrated in Fig. 5(b) and Fig. 6(b) for the hydrogenation and the dehydrogenation, respectively. The apparent activation energy of hydrogenation was calculated to be 65 kJ/mol, far lower than the ball-milled and cast $Mg_{90}Al_{10}$ alloy [36], and lower than 81 kJ/mol for the ball-milled MgH_2−10wt.%$Mg_{17}Al_{12}$ composite [20], but close to 65.5 kJ/mol for the Ni-catalyzed Mg−Al alloy [21]. For dehydrogenation, the apparent activation energy was 78 kJ/mol, close to that of the Nd-doped Mg−Al alloy [38], but far lower than 136 kJ/mol for the pure $Mg_{0.9}Al_{0.1}$ solid solution alloy [5] and 160 kJ/mol for pure Mg, and also lower than that of the Y_2O_3@graphene nano-composites catalyzed Mg−Al alloy [25]. However,

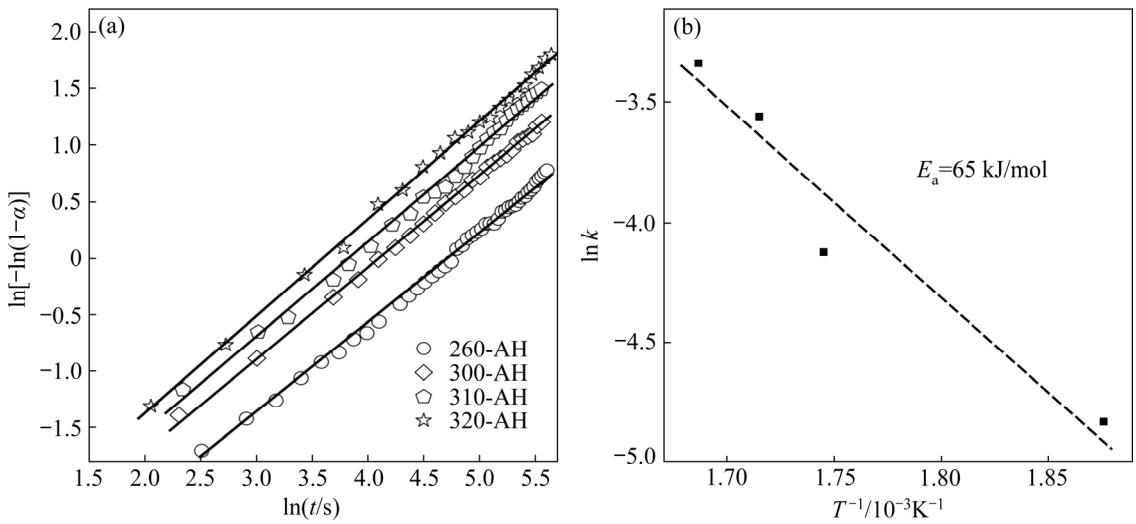

Fig. 5 Linear fitting plots of ln[−ln(1−α)] vs ln t for hydrogenation (a) and corresponding Arrhenius plot (b)

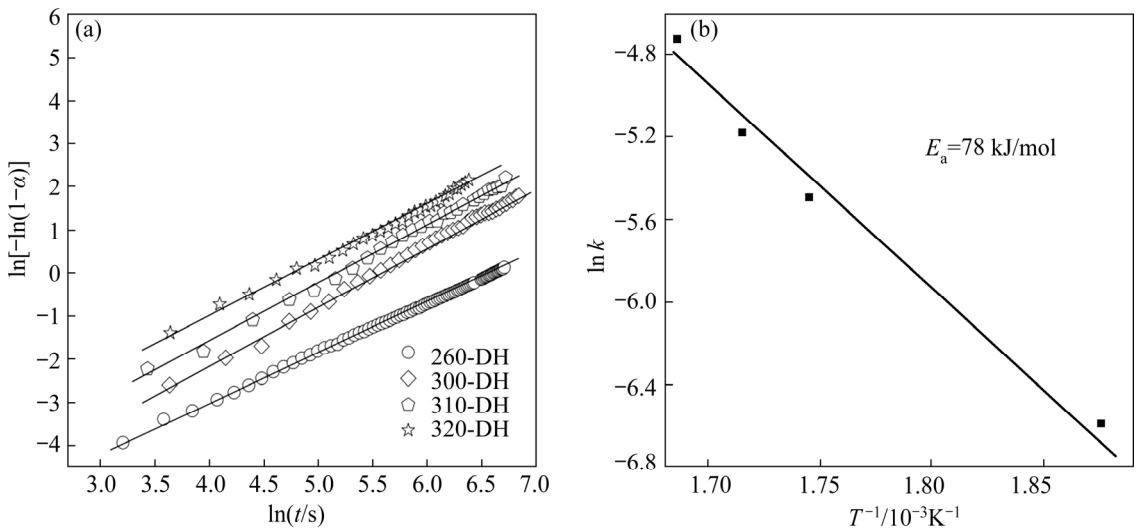

Fig. 6 Linear fitting plots of ln[−ln(1−α)] vs ln t for dehydrogenation (a) and corresponding Arrhenius plot (b)

YH_2/Y_2O_3 nanocomposite catalyzed Mg(Zn) solid solution alloy showed better dehydriding/hydriding kinetics than $Mg_{0.93}Al_{0.07}$−5wt.%LaF_3 nanocomposite [39].

The reaction exponent η values for hydrogenation were gotten to about 0.8, but approximately 1.9 for dehydrogenation in the present experimental temperature range. The variation of η values indicated different mechanisms of rate limitation for the dehydriding/hydriding reaction. The hydrogen absorption reaction could be controlled by one dimension diffusion rate of H atoms judged by η values. As we known, ball milling produces irregular submicron particle morphology and lots of defects, which benefits the nucleation of MgH_2. So, MgH_2 promptly nucleates on the surface of Mg particles, and randomly grows in three dimensions. When the surface of particles is rigidly covered by a layer of MgH_2, it is difficult for H atoms to diffuse to the inner of particles due to its small diffusion coefficient in MgH_2. Thus, the diffusion of H atoms becomes a rate limited step for the hydrogenation reaction. As shown in Fig. 4(a), a visible deceleration could be observed for the hydrogen absorption when hydrogen content reached about 50% ($\alpha > 0.5$). With respect to the hydrogen desorption reaction, the values of η were closer to 2, which indicated a kinetic mechanism of two-dimensional interface movement controlled reaction. Based on Refs. [17,35], the dehydrogenation/hydrogenation mode of Mg (nucleation and growth) could not be altered by the catalytic additives, but the additives or introduced phases could serve as nucleation sites for Mg. We know that the nucleation of Mg is very difficult and with a large energy barrier in pure MgH_2 [5,12,16,40]. However, for $Mg_{0.93}Al_{0.07}$−5wt.%LaF_3 nanocomposite, as discussed in Section 3.1, nanostructure $Al_{11}La_3$ and MgF_2 highly dispersing in the MgH_2 matrix produced large amounts of phase boundaries and interfaces, which could not only serve as nucleation sites for Mg, but also provide diffusion channel for hydrogen atoms. As a result, the dehydriding kinetics was remarkably improved. So, the S-shape character of the dehydrogenation curve disappeared for the $Mg_{0.93}Al_{0.07}$−5wt.%LaF_3 nanocomposite, which was attributed to the shortened dehydrogenation pregnant period of MgH_2. However, the movement of interface between Mg and MgH_2 was hardly promoted by $Al_{11}La_3$ and MgF_2. Therefore, it is reasonable to believe that dehydrogenation is controlled by the two-dimensional movement of interface between Mg and MgH_2.

Therefore, the addition of LaF_3 gave rise to the superior dehydriding/hydriding kinetics for Mg(Al) solid solution alloy by significantly lowering the dehydriding/hydriding activation energies. Combined with Refs. [27,35], it was believed that $Al_{11}La_3$ and MgF_2 acted as catalysts for the hydrogen absorption and desorption. It was reported that $Mg(H,F)_2$ phase could be formed in the dehydriding/hydriding process, which served as hydrogen atoms diffusion channel or hydrogen pump for the hydrogen absorption and desorption of Mg [41]. It was also thought that MgF_2 could impede the formation of MgO which is harmful to the absorption and dissociation of H_2 molecules. On the other hand, $Al_{11}La_3$ and MgF_2 provided nucleation sites for Mg/MgH_2, but inhibited their growth. As observed in Fig. 3, the sample maintained the nanostructure after hydrogen absorption and desorption cycles, which benefited the improvements of dehydriding/hydriding kinetics and cycling stability. In addition to those, the emergence of defects, boundaries and interfaces also had positive effects on the dehydriding/hydriding kinetics. The heterogeneous interfaces, such as interface between Mg/MgH_2 and $Al_{11}La_3$, producing lattice mismatch, provided extra energy for the nucleation of Mg and MgH_2, which was similar to the ball-milled Mg−Mn composite [42]. At last but not the least, it should also be pointed out that the Al species played an important role in the improvement of kinetics in the way of enhancing the thermal conductivity and the exothermic formation of Mg(Al) solid solution alloy. The formation of Mg(Al) solid solution would consume Mg, which could accelerate the decomposition of MgH_2.

3.3 Dehydriding/hydriding thermodynamics

Figure 7 shows the hydrogen absorption and desorption PCI curves of $Mg_{0.93}Al_{0.07}$−5wt.%LaF_3 nanocomposite. Compared with pure Mg and the un-doped Mg(Al) solid solution alloys [5], $Mg_{0.93}Al_{0.07}$−5wt.%LaF_3 nanocomposite showed a flatter plateau and smaller hydrogen absorption and desorption lag, which were mainly attributed to the improved dehydriding/hydriding kinetics. On the

other hand, there was only one visible plateau for dehydrogenation/hydrogenation, which was different from the previous reported un-doped Mg(Al) solid solution alloys [5], indicating the changed dehydriding/hydriding mechanism by the addition of LaF_3 as discussed above.

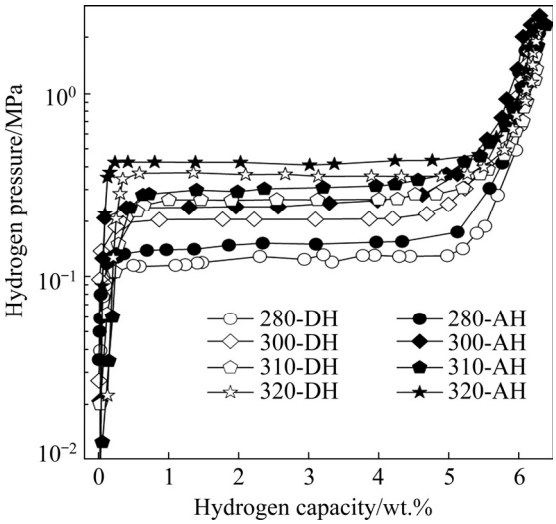

Fig. 7 PCI curves for $Mg_{0.93}Al_{0.07}$−5wt.%LaF_3 nano-composite at different temperatures

The varied dehydriding/hydriding mechanism generally results in the alteration of thermodynamics. To investigate the thermodynamics, the dehydriding/hydriding enthalpy and entropy were carefully calculated by van't Hoff method. The van't Hoff equation is expressed as follows:

$$\ln\left(\frac{P_{\text{eq.}}}{P_0}\right)=\frac{\Delta H}{RT}-\frac{\Delta S}{R} \tag{3}$$

where $P_{\text{eq.}}$ is the equilibrium plateau pressure (MPa), taken the pressure value of the midpoint at the dehydriding/hydriding plateau; P_0 is the standard atmospheric pressure (0.101 MPa), ΔH is the enthalpy change, and ΔS is the entropy change. In the present work, the hydrogen desorption plateau pressures at 280, 300, 310 and 320 °C were gotten together with the corresponding deviations, and illustrated in Fig. 8(a). The van't Hoff plot was gotten by fitting those equilibrium plateau pressure data using Eq. (3), and the results are illustrated in Fig. 8(b). The dehydriding enthalpy change (ΔH) and entropy change (ΔS) were achieved to be (69.7±1.9) kJ/mol and (127.9±3.4) J/(mol·K), respectively. The value of dehydriding enthalpy is very close to the previous reported 70.8 kJ/mol for the un-doped $Mg_{0.9}Al_{0.1}$ solid solution alloy [5], but

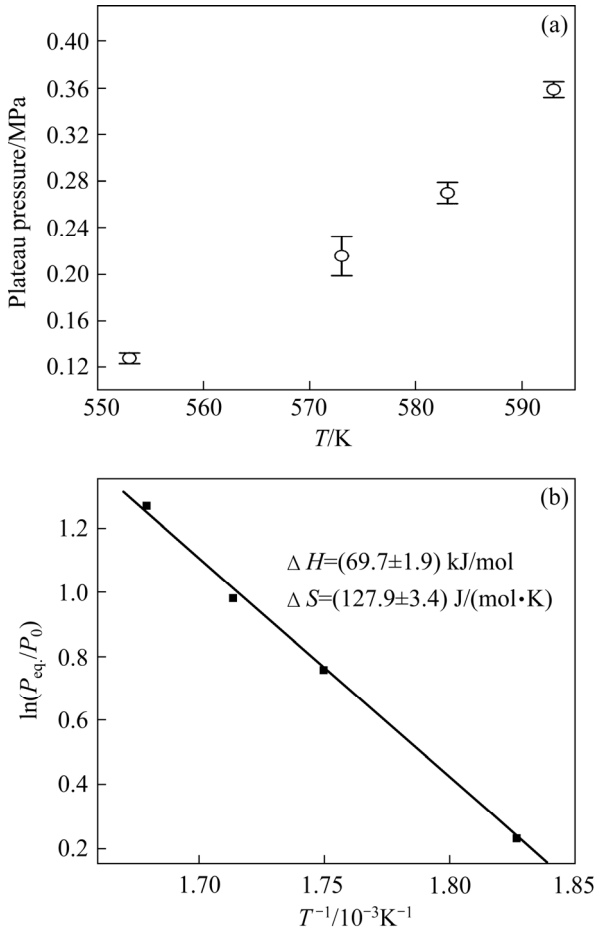

Fig. 8 Equilibrium plateau pressures at different temperatures (a) and van't Hoff plot (b)

lower than 77.9 kJ/mol for pure Mg [40]. Since the catalytic additives enhance the kinetics, but hardly change the thermodynamics. There must be other factors, except $Al_{11}La_3$ and MgF_2, resulting in the reduction of dehydriding enthalpy. The above phase transition analysis revealed that some element Al re-dissolved into Mg lattice, which was similar to the Mg(Al) solid solution alloy. The exothermic reaction of the formation of Mg(Al) solid solution alloy could compensate the endothermic dehydrogenation of MgH_2 in some degree. Also, it was reported that the dissolving of Al in the MgH_2 lattice would result in the destabilization of thermodynamics [43]. On the other hand, the multiphase and nanostructure giving rise to the extra interface interactions could also play an important role in the destabilization of MgH_2 [44,45]. But it was thought that the reaction of MgH_2 and Al forming Mg(Al) solid solution alloy was the main factor responsible for the lowered dehydriding enthalpy.

4 Conclusions

(1) $Mg_{0.93}Al_{0.07}$ solid solution alloy was prepared and LaF_3 was homogeneously added to synthesize a nanocomposite by ball milling.

(2) The dehydriding/hydriding mechanism of $Mg_{0.93}Al_{0.07}$ solid solution alloy is changed by the addition of LaF_3.

(3) The in situ formed nanostructure $Al_{11}La_3$ combining with MgF_2 takes positive effects on enhancing the hydrogen absorption and desorption of Mg, and blocks the growth of nano-Mg/MgH_2.

(4) The dual-modulation of the dehydriding/hydriding kinetics and thermodynamics is mainly attributed to the addition of LaF_3 and Al.

Acknowledgments

This work was financially supported by the National Natural Science Foundation of China (No. 51779103), the Natural Science Foundation of Fujian Province, China (No. 2021J011209), the Open Fund of Fujian Provincial Key Laboratory of Functional Materials and Applications (Xiamen University of Technology, fma2018007 and fma2020003), and Fujian Provincial Key Laboratory of Naval Architecture and Ocean Engineering (Jimei University), China.

References

[1] SCHLAPBACH L, ZŰTTEL A. Hydrogen-storage materials for mobile applications [J]. Nature, 2001, 414(6861): 353−358.

[2] LAI Q W, PASKEVICIUS M, SHEPPARD D A, BUCKLEY C E, THORNTON A W, HILL M R, GU Q F, MAO J F, HUANG Z G, LIU H K, GUO Z P, BANERJEE A, CHAKRABORTY S, AHUJA R, AGUEY-ZINSOU K F. Hydrogen storage materials for mobile and stationary applications: Current state of the art [J]. ChemSusChem, 2015, 8: 2789−2825.

[3] OUYANG L Z, LIU F, WANG H, LIU J W, YANG X S, SUN L X, ZHU M. Magnesium-based hydrogen storage compounds: A review [J]. Journal of Alloys and Compounds, 2020, 832: 154865.

[4] ZHONG H C, WANG H, LIU J W, SUN D L, ZHU M. Altered desorption enthalpy of MgH_2 by the reversible formation of Mg(In) solid solution [J]. Scripta Materialia, 2011, 65: 285−287.

[5] ZHONG H C, WANG H, OUYANG L Z. Improving the hydrogen storage properties of MgH_2 by reversibly forming Mg−Al solid solution alloys [J]. International Journal of Hydrogen Energy, 2014, 39: 3320−3326.

[6] ZHOU C S, BOWMAN R C Jr, FANG Z Z, LU J, XU L, SUN P, LIU H, WU H, LIU Y. Amorphous TiCu-based additives for improving hydrogen storage properties of magnesium hydride [J]. ACS Applied Materials & Interfaces, 2019, 11(42): 38868−38879.

[7] GAO S C, WANG X H, LIU H Z, HE T, WANG Y Y, LI S Q, YAN M. CNTs decorated with CoFeB as a dopant to remarkably improve the dehydrogenation rehydrogenation performance and cyclic stability of MgH_2 [J]. International Journal of Hydrogen Energy, 2020, 45(53): 28964−28973.

[8] XIA G L, TAN Y B, CHEN X W, SUN D L, GUO Z P, LIU H K, OUYANG L Z, ZHU M, YU X B. Monodisperse magnesium hydride nanoparticles uniformly self-assembled on graphene [J]. Advanced Materials, 2015, 27(39): 5981−5988.

[9] EDALATI K, UEHIRO R, IKEDA Y, LI H W, EMAMI H, FILINCHUK Y, ARITA M, SAUVAGE X, TANAKA I, AKIBA E, HORITA Z. Design and synthesis of a magnesium alloy for room temperature hydrogen storage [J]. Acta Materialia, 2018, 149: 88−96.

[10] ZHONG Hai-chang, XU Jin-bo, JIANG Chun-hai, LU Xiang-jun. Microstructure and remarkably improved hydrogen storage properties of Mg_2Ni alloys doped with metal elements of Al, Mn and Ti [J]. Transactions of Nonferrous Metals Society of China, 2018, 28: 2470−2477.

[11] ZHANG J G, ZHU Y F, LIN H J, LIU Y N, ZHANG Y, LI S Y, MA Z L, LI L Q. Metal hydride nanoparticles with ultrahigh structural stability and hydrogen storage activity derived from microencapsulated nanoconfinement [J]. Advanced Materials, 2017, 29: 1700760−1700765.

[12] WANG H, ZHONG H C, OUYANG L Z, LIU J W, SUN D L, ZHANG Q A, ZHU M. Fully reversible de/hydriding of Mg base solid solutions with reduced reaction enthalpy and enhanced kinetics [J]. The Journal of Physical and Chemistry C, 2014, 118 (23): 12087−12096.

[13] ZHONG H C, WANG H. Effects of indium on the dehydriding properties of MgH_2 [J]. Rare Metal Materials and Engineering, 2014, 43(11): 2806−2809. (in Chinese)

[14] REILLY J Jr, WISWALL R H Jr. The reaction of hydrogen with alloys of mangnesium and nickel and the formation of Mg_2NiH_4 [J]. Inorganic Chemistry, 1968, 7: 2254−2256.

[15] LI Zhen-yang, LI Sheng-li, YUAN Ze-ming, ZHANG Yang-huan, QI Yan. Microstructure, hydrogen storage thermodynamics and kinetics of $La_5Mg_{95-x}Ni_x$ (x=5, 10, 15) alloys [J]. Transactions of Nonferrous Metals Society of China, 2019, 29: 1057−1066.

[16] XIE Li-shuai, LI Jin-shan, ZHANG Tie-bang, KOU Hong-chao. Role of milling time and Ni content on dehydrogenation behavior of MgH_2/Ni composite [J]. Transactions of Nonferrous Metals Society of China, 2017, 27: 569−577.

[17] LIU T, QIN C G, ZHANG T W, CAO Y R, ZHU M, LI X G. Synthesis of Mg@$Mg_{17}Al_{12}$ ultrafine particles with superior hydrogen storage properties by hydrogen plasma-metal reaction [J]. Journal of Materials Chemistry, 2012, 22:

19831−19838.

[18] ZHU Y L, LUO S C, LIN H J, LIU Y N, ZHU Y F, ZHANG Y, LI L Q. Enhanced hydriding kinetics of Mg−10at.%Al composite by forming $Al_{12}Mg_{17}$ during hydriding combustion synthesis [J]. Journal of Alloys and Compounds, 2017, 712: 44−49.

[19] SHANG Hong-wei, LI Ya-qin, ZHANG Yang-huan, WEI Xin, QI Yan, ZHAO Dong-liang. Influence of adding nano-graphite powders on the microstructure and gas hydrogen storage properties of ball-milled $Mg_{90}Al_{10}$ alloys [J]. Carbon, 2019, 149: 93−104.

[20] ANDREASEN A. Hydrogenation properties of Mg−Al alloys [J]. International Journal of Hydrogen Energy, 2008, 33: 7489−7497.

[21] LI S J, ZHU Y F, LIU Y N, ZHANG Y, LIN H J, ZHANG J G, QIU W J, LI L Q. Nano-inducement of Ni for low-temperature dominant dehydrogenation of Mg−Al alloy prepared by HCS+MM [J]. Journal of Alloys and Compounds, 2020, 819: 153020-9.

[22] LIANG G, HUOT J, BOILY S, NESTE A V, SCHULZ R. Catalytic effect of transition metals on hydrogen sorption in nanocrystalline ball milled MgH_2−Tm (Tm=Ti, V, Mn, Fe and Ni) systems [J]. Journal of Alloys and Compounds, 1999, 292: 247−252.

[23] HE T, WANG X H, LIU H Z, GAO S C, WANG Y Y, LI S Q, YAN M. Enhanced hydrogen desorption/absorption properties of magnesium hydride with CeF_3@Gn [J]. International Journal of Hydrogen Energy, 2020, 45(7): 4754−4764.

[24] DANAIE M, MITLIN D. TEM analysis of the microstructure in TiF_3-catalyzed and pure MgH_2 during the hydrogen storage cycling [J]. Acta Materialia, 2012, 60: 6441−6456.

[25] LAN Z Q, SUN Z Z, DING Y C, NING H, WEI W L, GUO J. Catalytic action of Y_2O_3@graphene nanocomposites on the hydrogen-storage properties of Mg−Al alloys [J]. Journal of Materials Chemistry A, 2017, 5(29): 15200−15207.

[26] WANG J S, LI Y, LIU T, PENG D D, HAN S M. Synthesis of Mg-based composite material with in-situ formed LaH_3 and its hydrogen storage characteristics [J]. Journal of Rare Earths, 2018, 36(7): 739−744.

[27] ZHOU C Q, LI C, LI Y T, ZHANG Q A. Enhanced hydrogen storage kinetics of an Mg−Pr−Al composite by in situ formed Pr_3Al_{11} nanoparticles [J]. Dalton Transactions, 2019, 48(22): 7735−7742.

[28] HUOT J, PELLETIER J F, LURIO L B, SUTTON M, SCHULZ R. Investigation of dehydrogenation mechanism of MgH_2−Nb nanocomposites [J]. Journal of Alloys and Compounds, 2003, 348: 319−324.

[29] HANADA N, ICHIKAWA T, FUJII H. Catalytic effect of nanoparticle 3d-transition metals on hydrogen storage properties in magnesium hydride MgH_2 prepared by mechanical milling [J]. The Journal of Physical Chemistry B, 2005, 109(15): 7188−7194.

[30] SONG M Y, BOBET J L, DARRIET B. Improvement in hydrogen sorption properties of Mg by reactive mechanical grinding with Cr_2O_3, Al_2O_3 and CeO_2 [J]. Journal of Alloys and Compounds, 2002, 340: 256−262.

[31] PAN Yin-cheng, ZOU Jian-xin, ZENG Xiao-qin, DING Wen-jiang. Hydrogen storage properties of Mg−TiO_2 composite powder prepared by arc plasma method [J]. Transactions of Nonferrous Metals Society of China, 2014, 24: 3834−3839.

[32] CUI J, WANG H, LIU J W, OUYANG L Z, ZHANG Q A, SUN D L, YAO X D, ZHU M. Remarkable enhancement in dehydrogenation of MgH_2 by a nano-coating of multi-valence Ti-based catalysts [J]. Journal of Materials Chemistry A, 2013, 18: 5603-11.

[33] ZHANG H W, ZHENG X Y, WANG T, LI X G. Significantly improved hydrogen desorption property of La_2Mg_{17} alloy modified with Ni−Al nanocrystalline [J]. Intermetallics, 2016, 70: 29−32.

[34] XIE X B, LI Y C, CHEN M, HU M M, FENG Y X, SHANG J X, LIU T. Catalytic effects of decorating AlV_3 nanocatalyst on hydrogen storage performance of Mg@$Mg_{17}Al_{12}$ nanocomposite: Experimental and theoretical study [J]. ACS Sustainable Chemistry & Engineer, 2020, 8: 4920−4930.

[35] PANG Y P, YUAN T, YANG J H, GAO M X, PAN H G, LIU Y F, ZHENG S Y. In situ formation of Al_3Ti, MgF_2 and Al and their superior synergetic effects on reversible hydrogen storage of MgH_2 [J]. Catalysis Today, 2018, 318: 107−112.

[36] LI Ya-qin, ZHANG Yang-huan, SHANG Hong-wei, QI Yan, LI Ping, ZHAO Dong-liang. Investigation on structure and hydrogen storage performance of as-milled and cast $Mg_{90}Al_{10}$ alloys [J]. International Journal of Hydrogen Energy, 2018, 43: 6642−6653.

[37] LI Ya-qin, ZHANG Yang-huan, SHANG Hong-wei, QI Yan, LI Ping, ZHAO Dong-liang. Effects of adding nano-CeO_2 powder on microstructure and hydrogen storage performances of mechanical alloyed $Mg_{90}Al_{10}$ alloy [J]. International Journal of Hydrogen Energy, 2019, 44: 1735−1749.

[38] LI Ya-qin, SHANG Hong-wei, TIAN Jun-long, ZHANG Yang-huan, ZHANG Xi-wei, TANG Zhen-jie, ZHANG Ya-tao. Effects of adding Nd on the microstructure and dehydrogenation performance of $Mg_{90}Al_{10}$ alloy [J]. Materials Characterization, 2021, 171: 110795-13.

[39] ZHONG H C, HUANG Y S, DU Z Y, LIN H J, LU X J, CAO C Y, CHEN J H, DAI L Y. Enhanced hydrogen Ab/De-sorption of Mg(Zn) solid solution alloy catalyzed by YH_2/Y_2O_3 nanocomposite [J]. International Journal of Hydrogen Energy, 2020, 45(51): 27404−27412.

[40] ZHONG H C, WANG H, OUYANG L Z, ZHU M. Microstructure and hydrogen storage properties of Mg−Sn nanocomposite by mechanical milling [J]. Journal of Alloys and Compounds, 2011, 509: 4268−4272.

[41] YOUN J S, PHAN D T, PARK C M, JEON K J. Enhancement of hydrogen sorption properties of MgH_2 with a MgF_2 catalyst [J]. International Journal of Hydrogen energy, 2017, 42: 20120−20124.

[42] LU Y S, KIM H, SAKAKI K, HAYASHI S, JIMURA K, ASANO K. Destabilizing the dehydrogenation thermodynamics of magnesium hydride by utilizing the

immiscibility of Mn with Mg [J]. Inorganic Chemistry, 2019, 58(21): 14600−14607.

[43] VERMEULEN P, van THIEL E F M J, NOTTEN P H L. Ternary $MgTi_x$-alloys: A promising route towards low-temperature, high-capacity, hydrogen-storage materials [J]. Chemistry—A European Journal, 2007, 13: 9892−9898.

[44] BALDI A, MOOIJ L, PALMISANO V, SCHREUDERS H, KRISHNAN G, KOOI B J, DAM B, GRIESSEN R. Elastic versus alloying effects in Mg-based hydride films [J]. Physical Review Letters, 2018, 121: 255503-7.

[45] PATELLI N, MIGLIORI A, MORANDI V, PASQUINI L. Interfaces within biphasic nanoparticles give a boost to magnesium-based hydrogen storage [J]. Nano Energy, 2020, 72: 104654−10.

球磨添加 LaF_3 的 Mg(Al)固溶体合金的储氢性能

钟海长[1]，林晨龙[1]，杜子宇[1]，曹春燕[1]，梁 初[2]，郑青榕[3]，戴乐阳[3]

1. 厦门理工学院 材料科学与工程学院 福建省功能材料与应用重点实验室，厦门 361024；
2. 浙江工业大学 材料科学与工程学院，杭州 310014；
3. 集美大学 轮机工程学院 福建省船舶与海洋工程重点实验室，厦门 361021

摘 要：通过球磨添加 LaF_3 促进 Mg(Al)固溶体合金的吸/放氢过程。利用 XRD 技术分析样品的相组成和吸/放氢过程的相转变。采用扫描电镜(SEM)和扫描透射电镜(STEM)观察样品的显微组织和相分布。采用 Sieverts 方法对样品的储氢性能进行测试。$Mg_{0.93}Al_{0.07}$−5%LaF_3(质量分数)纳米复合物的吸氢反应激活能和脱氢反应激活能分别降低至 65 和 78 kJ/mol，从而使其吸/放氢动力学性能得到显著提高，其脱氢反应焓为 69.7 kJ/mol。复合物储氢性能的改善主要归因于铝固溶到镁晶格中以及原位生成纳米结构 $Al_{11}La_3$ 和 MgF_2 的催化作用。

关键词：三氟化镧；氢化镁；镁；铝；储氢性能；氢化

(Edited by Wei-ping CHEN)